THE JOURNAL OF PHYSICAL CHEMISTRY A

Article

pubs.acs.org/JPCA

Extraordinary Mechanism of the Diels–Alder Reaction: Investigation of Stereochemistry, Charge Transfer, Charge Polarization, and Biradicaloid Formation

Thomas Sexton, Elfi Kraka, and Dieter Cremer*

Computational and Theoretical Chemistry Group (CATCO), Department of Chemistry, Southern Methodist University, 3215 Daniel Avenue, Dallas, Texas 75275-0314, United States

Supporting Information

ABSTRACT: The Diels–Alder reaction between 1,3-butadiene and ethene is investigated from far-out in the entrance channel to the very last step in the exit channel thus passing two bifurcation points and extending the range of the reaction valley studied with URVA (Unified Reaction Valley Approach) by 300% compared to previous studies. For the first time, the pre- and postchemical steps of the reaction are analyzed at the same level of theory as the actual chemical processes utilizing the path curvature and its decomposition into internal coordinate or curvilinear coordinate components. A first smaller charge transfer to the dienophile facilitates the rotation of gauche butadiene into its cis form. The actual chemical processes are initiated by a second larger charge transfer to the dienophile that facilitates pyramidalization of the reacting carbon centers, bond equalization, and biradicaloid formation of the reactants. The transition state is aromatically stabilized and moved by five path units into the entrance channel in line with the Hammond–Leffler postulate. The pseudorotation of the boat form into the halfchair of cyclohexene is analyzed. Predictions are made for the Diels–Alder reaction based on a 11-phase mechanism obtained by the URVA analysis.

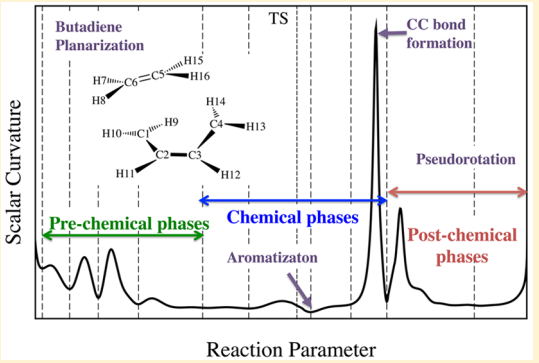

1. INTRODUCTION

The Diels–Alder (DA) reaction is one of the most applied and best investigated synthetic methods in chemistry[1−5] because of its relatively low reaction barrier,[6−8] the versatility of the parent noncatalyzed version, its acceleration by Lewis-acid catalysts,[3,9−13] or the possibilities provided by the retro-DA,[14−16] and the hetero-DA reaction.[1,2] In the DA reaction, a diene such as 1,3-butadiene (BD) undergoes a cycloaddition with a dienophile such as ethene (E), which implies that three π-bonds are broken and two new σ- and one new π-bond are formed. Apart from these chemical processes, there are important pre- and postchemical processes that have to take place in the reaction complex (RC) to make the cycloaddition possible. For the parent DA reaction (Figure 1), BD has to rotate from the preferred anti (s-trans) form into the less populated gauche form.[17] Then, gauche-BD has to be forced into a planar syn-form to establish the new CC bonds between the reactants via π,π-overlap. For the retro-DA, the stable halfchair form of cyclohexene has to convert into a boat form via ring pseudorotation.[18] These pre- and postchemical processes have an impact on the energetics, the stereochemistry, and the mechanism of the DA reaction, but are generally ignored as not important conformational processes of the RC.

The energetics and dynamics of the parent DA reaction have been studied both experimentally and computationally[5,6,8,19−23] where in the latter investigations a comparison between concerted and nonconcerted reaction was made. The necessity of understanding the mechanism of the DA reaction has been the motivation for a multitude of conceptual investigations.[5,24−31] One important result of these studies was the description of the transition state (TS) of the DA reaction as being Hückel-aromatic.[25,31−37]

Most computational investigations of the parent DA reaction focused on the stationary points of the reaction path (reactants, TS, product) in the sense of a conventional mechanistic study. Only a few exceptions can be found in the literature, in which the RC is followed along the reaction path and analyzed with regard to its electronic structure changes.[29,30,34] Among these computational studies, the work of Kraka and co-workers[34] is of special interest because it derived the mechanism of the DA reaction directly from features of the potential energy surface (PES) of the RC by following the reaction from the entrance valley via the TS to the exit valley utilizing the Unified Reaction Valley Approach (URVA).[38−40] Since the floor line of the reaction valley is curved at those positions where bond breaking/forming or other electronic changes occur, they could identify, by calculating the curvature of the reaction path, three regions of electronic structure changes, which they associated with a charge transfer, spin-recoupling, and bond formation step. Their work led to a distinction between symmetry-allowed and

Received: November 24, 2015
Revised: January 18, 2016
Published: January 19, 2016

ACS Publications © 2016 American Chemical Society

DOI: 10.1021/acs.jpca.5b11493
J. Phys. Chem. A 2016, 120, 1097−1111

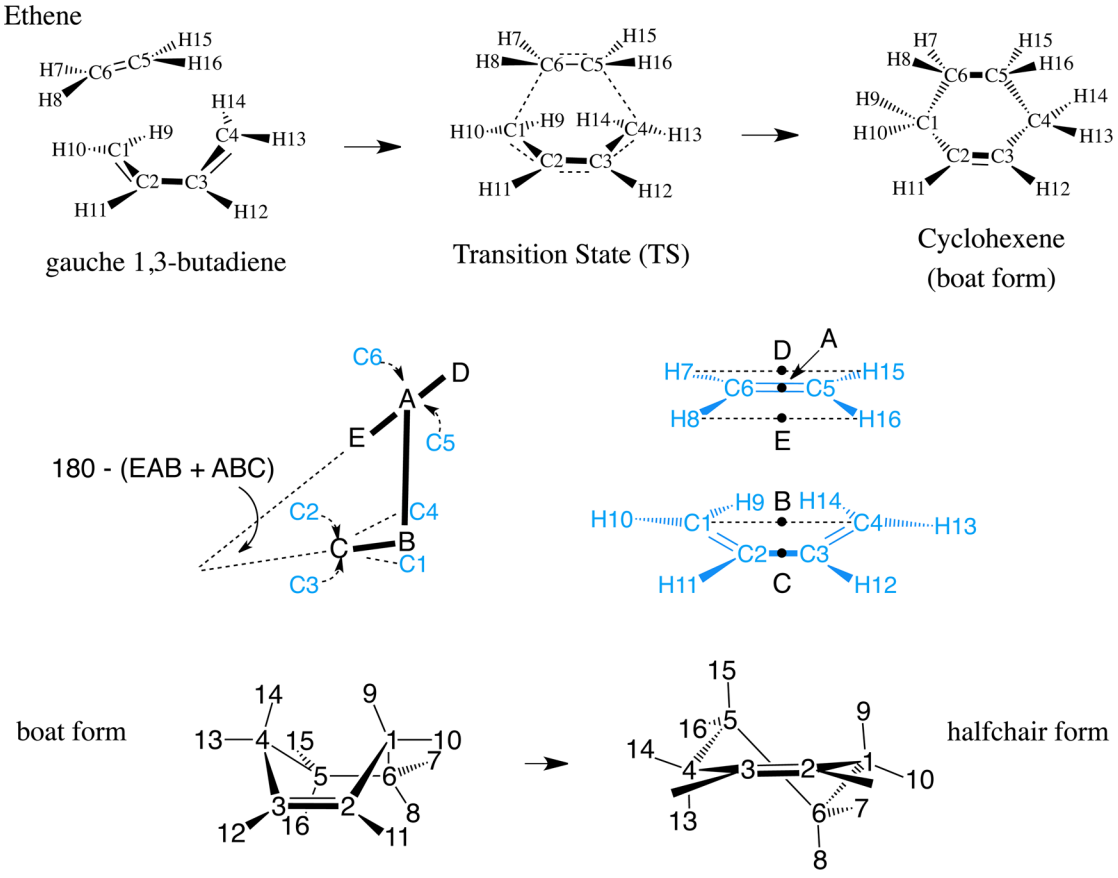

Figure 1. Diels–Alder reaction between 1,3-butadiene and ethene leading to cyclohexene: Numbering of atoms. Also given is a geometric model describing the approach of the two reactants (see text) and the boat and halfchair form of cyclohexene.

symmetry-forbidden pericyclic reactions based on the dynamics of the RC,[39] the identification of hidden TSs and hidden intermediates typical of forbidden reactions,[39,41] and a relation of each reaction step to a distinct change in the RC via the curvature coupling coefficients based on local vibrational modes.[38,40,42]

This previous work based on the reaction valley of the parent DA reaction and the URVA method (URVA03)[40,43,44] was hampered by the fact that the algorithm used could not follow the reaction valley and the curving reaction path into those regions where the reactants first meet and the stereochemistry of the reaction is decided. The accessible reaction valley was limited by stationary points in form of path-bifurcation points, beyond which the flatness of the valley made a following of its floor line difficult.

With this work, we present a strongly improved URVA method (URVA15)[45] by which the previous investigation of the reaction valley of the parent DA reaction can be extended by 300% thus including not only the region where the chemical processes take place but also those regions where in the pre- and postchemical processes (*reaction phases* in the terminology of URVA[39,40]) the stereochemistry of the (retro) DA reaction is decided. Two path bifurcation points are detected in the entrance and exit valley. Using an advanced reaction path following algorithm one branch of the valley is traced beyond these bifurcation points. Apart from this, we base the analysis on both internal and curvilinear coordinates where the latter provide a better means to describe changes in the RC in certain valley regions. In this way, the URVA reinvestigation of the parent DA reaction can provide answers to a number of mechanistic questions, which previously could not be answered.[34]

(1) The RC starts with a C_1-symmetrical structure. What form does this have and what forces are responsible for this form? (2) Previous studies showed that reaction phases are closely related to specific electronic structure changes associated with distinct curvature changes of the reaction path.[39,40,43,44] Conformational changes of the RC should not lead to any curvature changes because they only involve small electronic structure changes. Does this also hold for the electronic structure changes of the RC during the DA reaction? Are the pre- and postchemical regions mechanistically (not) relevant? (3) Several investigations have indicated that the fate of the RC is often decided in the van der Waals region.[41,46−49] Does this also hold in the case of the DA reaction? (4) Similar considerations apply to the electronic structure changes of the RC in the exit channel of the reaction valley. Cyclohexene is formed in its boat conformation. Its most stable form is the halfchair conformation.[50] Can one follow the reaction valley to the halfchair form and get in this way any information, which may be relevant for the retro-DA reaction? (5) The DA reaction is known to be catalyzed in water by enforced hydrophobicity.[51−53] Can URVA verify and quantify the existing models for water catalysis in the case of the parent DA reaction? (6) Is there any other possibility of catalyzing the parent DA reaction? (7) The orbital analysis of the DA reaction of many dienes and dienophiles has been extremely successful. Can one explain this success from the more general point of view provided by the URVA analysis? (8) What makes the mechanism of symmetry-allowed pericyclic reactions so special? (9) What general insights can be gained by being able to

DOI: 10.1021/acs.jpca.5b11493
J. Phys. Chem. A 2016, 120, 1097−1111

investigate a chemical reaction far out into the entrance and exit channel?

The results of this investigation are presented in the following way. In section 2, the computational methods employed in this work are summarized. Results and discussions are presented in section 3. Section 4 contains the conclusions of this work.

2. COMPUTATIONAL METHODS

URVA is based on the Reaction Path Hamiltonian of Miller, Handy, and Adams[54] and the local vibrational mode description of Konkoli and Cremer.[42,55−57] The basics of the URVA method have been described in several review articles[39,40,43,44] and therefore we refrain from a detailed description of the basis of URVA.

In this and other work, URVA is based on a dual level approach: The stationary points along the reaction path are calculated with CCSD(T)[58] using Dunning's cc-pVTZ basis set[59] to determine the energetics of the reaction as accurate as possible. The reaction valley and the reaction path are calculated at the DFT level because previous work has shown that this is sufficient in most cases. In this work, we have used B3LYP[60−62] in combination with Pople's 6-31G(d,p) basis set[62] because this hybrid XC functional turns out to be robust especially when the third order response properties in terms of the curvature coupling coefficients (see below) have to be calculated. In addition, we used the ωB97X-D functional,[63,64] which includes long-range Hartree−Fock (HF) exchange for suppressing self-interaction errors, some short-range HF exchange for a better description of the exchange hole, and Lennard-Jones-type corrections to ensure a better description of dispersion interactions. Both XC functionals were used for the URVA description and for converting ΔE values (ΔE^a, ΔE_R: activation and reaction energies) into the corresponding enthalpies at 298 K, $\Delta H(298)$, and free energies at 298 K, $\Delta G(298)$, with the help of calculated thermochemical corrections. Basis set superposition errors (BSSE) were corrected using the counterpoise method.[65]

URVA requires a representative path, which in this work is chosen to be the valley floor line. This is given by the IRC (intrinsic reaction coordinate) path of Fukui.[66] However, any other representative path, e.g., a downhill path from an energy plateau in the case of a barrierless reaction, can also be used[46,67] and insofar URVA is not limited to reactions with a TS. The reaction valley is spanned by $3N - L - 1$ normal coordinates (N, number of atoms; L, number of translations and rotations; 1 additional translation along the reaction path), which *lead* the harmonic vibrational modes of the RC orthogonal to the path; i.e., the reaction valley is described in the harmonic approximation.

The *reaction path coordinate* is given by the mass-weighted vector $\tilde{\mathbf{x}}(s)$ where the arc length s of the path is measured in amu$^{1/2}$ Bohr (amu: atomic mass units; for reasons of brevity we will use the term *s-units*). The arc length s is set equal to zero at the TS. It is negative in the entrance channel (reactant side) and positive in the exit channel (product side). The walk along the reaction path was made in steps of 0.03 *s*-units. In total 1020 path points were calculated from −16.6 to +14.0 *s*-units (range of the previous investigation: −3.8 to +6.0 *s*-units; in the range −6.8 to −3.8 *s*-units, the path curvature became erratic[34]). In each case, an ultrafine grid and tight convergence criteria for the geometry optimization of the RC following the path were used. The path following algorithm was set up to pass bifurcation points in entrance and exit channel. The results of these investigations were verified by additional URVA calculations that started at a bifurcation point (in the entrance channel, indicated by the appearance of a valley ridge inflection point (VRI) and the conversion of one frequency into an imaginary frequency) and followed one of the valleys out into the van der Waals region.

In the exit channel at the bifurcation point, the RC adopts a boat conformation of cyclohexene. The path starting at this point is associated with the ring conversion to the cyclohexene half-chair conformation. In the entrance channel, the path continues past a valley ridge inflection point, but falls off of one side of the ridge before the bifurcation point is reached. However, locating the entrance channel bifurcation point is still possible based on a TS search starting from the point where the imaginary frequency is greatest.

At each path point, the gradient and the Hessian of the RC are calculated to determine the path direction vector $\boldsymbol{\eta}(s)$ and the scalar path curvature $\kappa(s)$ (length of the curvature vector $\boldsymbol{\kappa}(s)$, which must not be confused with the curvature of the energy profile $E(s)$ along the reaction path). They are calculated as first and second derivatives of $\tilde{\mathbf{x}}(s)$ in mass-weighted coordinates with regard to s after projecting out translations and rotations of the RC (for details, see ref 38). The vector $\boldsymbol{\eta}(s)$ and the scalar $\kappa(s)$ are expressed in terms of the Konkoli−Cremer local vibrational modes $\mathbf{a}(s)$ and local curvature coupling coefficients $A_{n,s}(s)$ for internal coordinate $p_n(s)$ or, alternatively, in terms of the internal coordinate components $k_n(s)$,[45] which facilitate the analysis of the path direction and the curvature in cases of path instabilities. A positive (negative) curvature component indicates support of (resistance to) a given electronic structure change. The local and normal mode curvature coupling coefficients, $A_{n,s}(s)$ and $B_{\mu,s}(s)$ ($\mathbf{l}_\mu(s)$ is one of the $3N - (L + 1)$ normal modes with frequency ω_μ), are more adequate to analyze the dynamics of the RC because they describe the coupling of the vibrations with the translational mode and thereby energy transfer processes.[43,44,54] However, they become useless at path points where the valley frequencies turn out to be imaginary (e.g., in case of ridge paths), and therefore, they were only used to confirm and complement the information obtained by the internal coordinate components of the scalar curvature.

Electronic structure changes always imply a curving of the reaction path in the $3N - L$ configurational space.[39,40,43] If the path were a straight line, the forces exerted on the RC would change linearly, which is typical for electrostatically driven processes. Regions where distinct electronic structure changes take place in connection with rehybridization, charge transfer and polarization, bond cleavage or bond formation, changes in electron delocalization, etc. imply smaller or larger curvature enhancements and peaks where the width of a peak and peak ratios are directly related to the energetics of a process.[48] A curvature minimum indicates that the RC undergoes only minimal or linear changes and therefore it is useful to define a reaction phase as the path (valley) region from one $\kappa(s)$ minimum M_i to the next minimum M_{i+1} for increasing s; i.e., the reaction mechanism is described in a sequence of reaction phases.[39,40,43] Using the curvature components and/or the local curvature coupling coefficients, it is easy to find those curvature components $k_n(s)$ or curvature coupling coefficients $A_{n,s}(s)$, which cause the curvature peak, and, with the help of the associated internal coordinates $p_n(s)$, the electronic structure

DOI: 10.1021/acs.jpca.5b11493
J. Phys. Chem. A 2016, 120, 1097−1111

change responsible for the curvature enhancement or peak can be identified.

Often an analysis of $\boldsymbol{\eta}(s)$ in terms of its components leads to complementary information as it indicates which internal coordinates drive the reaction along the path, whereas the components of the curvature vector $\boldsymbol{\kappa}(s)$ (which is orthogonal to $\boldsymbol{\eta}(s)$) are related to the vibrational modes, which are associated with a change in the path direction and thereby with the electronic structure change enforcing the path to change its direction. Hence, a large contribution of a p_n-component to $\boldsymbol{\eta}(s)$ implies a small p_n-component contribution to $\boldsymbol{\kappa}(s)$ and vice versa. Contrary to the previous work on the DA reaction,[34] the analysis of $\boldsymbol{\kappa}(s)$ in this work is no longer carried out in terms of dynamically defined local modes **a** but geometrically based local modes **u**, which are derived from the mass-scaled vectors of the **B**-matrix.[45] In this way, the analysis becomes more robust with regard to path instabilities caused by failures of the quantum chemical method used, numerical errors, or the topology of the PES.[45]

The standard Euler predictor corrector and Hessian-based predictor−corrector methods used for IRC following often lead to erroneous path descriptions when reaching flat PES regions where the *E*-gradient is small.[68−71] To avoid these deficiencies, the predictor−corrector algorithm was improved by including third order terms in the Taylor expansion and applying an extended weighting function for fitting the PES along the line between two path points.[72] This turned out to be an important and cost-effective improvement of the reaction path following algorithm.

For each reaction phase discussed in this work, the percentage of energy consumption with regard to the energy barrier is given. Charge transfer and charge polarization was calculated from NBO (natural bond orbital) charges.[73,74] The changes of specific internal coordinates p_n, pyramidalization angles $\theta_{P,n}$, and curvilinear ring coordinates (puckering coordinates q_n, ϕ_n and deformation coordinates t_n,τ_n; in each case, an amplitude and a pseudorotation phase angle) were also monitored along the reaction path using the Cremer−Pople or Zou−Cremer algorithms.[18,75]

All calculations were carried out with the program packages COLOGNE15[76] (URVA calculations), MOLPRO[77] (coupled cluster calculations), and Gaussian09[78] (DFT calculations).

3. RESULTS AND DISCUSSION

In Table 1, the energetics of the DA reaction as calculated in this work is compared to that based on measured enthalpies and other calculations.[79] The energy profile calculated is shown in Figure 2 together with the reaction phases derived from the scalar curvature diagram of Figure 3. In total, 11 reaction phases can be distinguished (Figure 3) of which the first four determine the stereochemistry of the RC driven by the long-range interactions between the reactants, in phases 5 and 6, the reactants prepare for the reaction, and the chemical processes take place in phases 7, 8, and 9 whereas the conformational adjustment of the product formation takes place in the last three reaction phases.

Table 1. Themochemistry for the DA-reaction of E and BD.[a]

	ΔE^a	ΔE_R	$\Delta H^a(298)$	$\Delta H_R(298)$
B3LYP	23.4	−41.2	24.4	−36.8
CCSD(T)	22.4	−44.9	23.4	−40.5
CBS-QB3			21.5	−40.3
exp			24.8	−39.6

[a]All values in kcal/mol given with regard to the energy of anti = *s-trans*-1,3-butadiene. B3LYP/6-31G(d,p) with BSSE correction from the first point in the entrance channel. CCSD(T)/cc-pVTZ//ωB97-XD/aug-cc-pVTZ. Experimental activation enthalpy ΔH^a from ref 6, experimental ΔH_R from ref 81, and CBS-QB3 data from ref 79.

Energetics of the Diels−Alder Reaction. At the CCSD(T)/cc-pVTZ level of theory (using ωB97X-D) geometries), a barrier value ΔE^a of 22.4 kcal/mol and a reaction energy ΔE_R of −44.9 kcal/mol is obtained corresponding to enthalpies of 23.4 and −40.5 kcal/mol (see Table 1). Lischka and co-workers carried out MR-AQCC calculations to determine the reliable barrier values for the concerted and nonconcerted (via a biradical intermediate) parent DA reaction.[8] They report an energy barrier of 22.2 kcal/mol and a reaction energy of −39.7 kcal/mol, which correspond to enthalpy values $\Delta H^a(298)$ = 23.1 and $\Delta H_R(298)$ = −35.5 kcal/mol (experimental values: 27.5 (760−920 K);[6] 23.3 (0 K);[80] −39.6 (298 K)[81]). The nonconcerted transition state (TS) is 6.5 kcal/mol higher in energy.[8] Hu and co-workers carried out a dual-level direct dynamics study, calculated kinetic isotope effects, and investigated the impact of tunneling.[23] The performance of a large number of quantum chemical methods was studied by Gayatri, which included also B3LYP.[20] According to this study, DFT results, when carried out with a hybrid functional such as B3LYP, were close to CCSD(T) results.

A reliable account of the energetics of the parent DA reaction can be given with the dual level approach chosen in this work. Commonly and also in Table 1, the energetics of the reaction is given with regard to the *s-trans* (=anti) form of BD + E. Since the reaction valley is followed in this work from an entrance point starting at the gauche BD form, all energy differences are discussed in the following with regard to gauche BD + E.

Prechemical Processes (Reaction Phases 1−5). These include the long distance approach of the two reactants where BD reacts with its gauche conformation (C1C2C3C4:31°, Figure 1) that occupies a local minimum 3.1 kcal/mol higher in energy than that of the s-trans form and that can be populated after surmounting a barrier of 5.7 kcal/mol.[17] E approaches gauche BD by bridging the C1C4 distance and tilting its endo side toward BD so that its positively charged atoms H8 and H16 (Figure 1) can be attracted by the π-densities at C1 and C4. At s = −16.6 units, these distances are 3.09 and 3.16 Å and by this well outside the van der Waals distance of 1.8 + 1.2 = 3.0 Å[82] but still much closer than the distance between the C5C6 midpoint A and the C1C4 midpoint B (3.93 Å, Figure 1, Table 2). The tilting angle EAB (Figure 1, Table 2) is 21.3° indicating that exchange repulsion between the π-systems is partly avoided. The projection of the C5C6 bond of E onto the mean plane of BD is rotated by 5.7° (angle EABC, Figure 1, Table 1) toward C2 relative to the C2C3 axis to increase the attraction between H8 and C1. E is still somewhat outside the C1C4 connection line; i.e., it slides with its inclined (because of the gauche form of BD) and tilted orientation sidewards over BD driven by H,C attractive electrostatic forces. Bonding between the reactants would not be possible in this configuration of the RC.

In the first phase, E increases its tilting angle EAB slightly and starts to reorient relative to BD. This reorientations lasts for the first 4 phases: In phases 2 and 3, E rotates 5.4° where the RC is strongly resisting this rotation as is indicated by a

DOI: 10.1021/acs.jpca.5b11493
J. Phys. Chem. A 2016, 120, 1097−1111

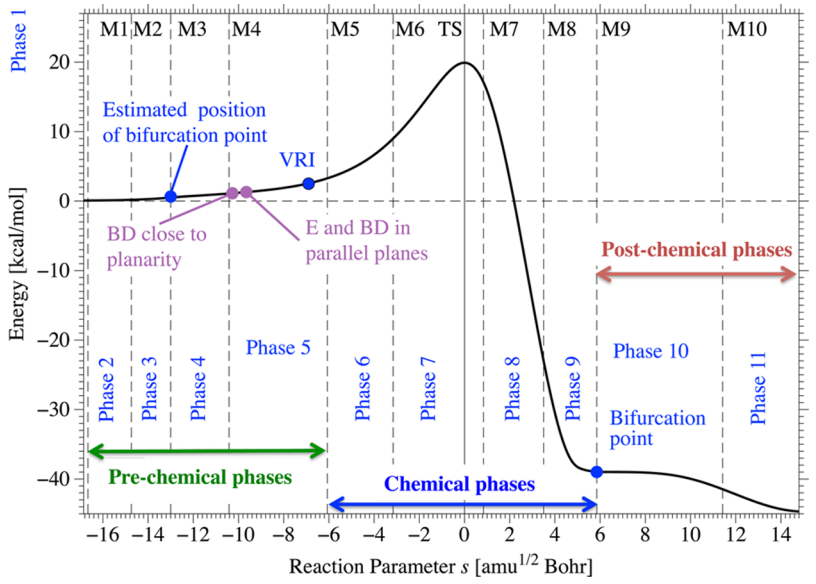

Figure 2. Energy diagram of the Diels–Alder reaction between 1,3-butadiene and ethene. The TS (vertical line) defines the zero point of the path parameter *s*. The entrance channel of the reaction is given by negative, the exit channel by positive *s* values. The 11 reaction phases are indicated and the curvature minima M1 to M10. The first 5 phases determine the prechemical, phases 6–9 the chemical, and phases 10 and 11 the postchemical reaction regions. The position of a path bifurcation point in the entrance channel (estimated) and the exit channel (exact) is also indicated. The VRI (valley ridge inflection point) determines the start of the side-valleys and a ridge path in the direction of more negative *s*-values. See text.

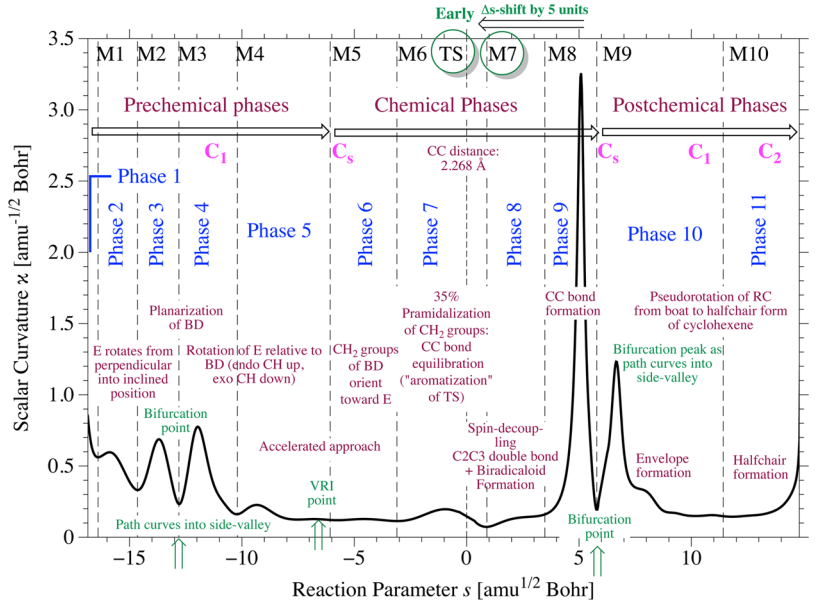

Figure 3. Curvature diagram of the Diels–Alder reaction between 1,3-butadiene and ethene. The 11 reaction phases as determined by the curvature minima M1 to M10 (indicated by dashed vertical lines) are shown. For each phase the dominant process is given. Also indicated are path specific features such as VRI (valley ridge inflection point), bifurcation points, and the early character of the TS.

negative curvature component (black dashed component C2C1C6C5 in Figure 4) because this rotation leads to increasing π,π-exchange repulsion. Bond C3C4 of BD is pushed down by the repulsion force where this force is increased by the continuing rotation of E at its C5C6 axis and a decreasing distance AB.

The curvatures peaks in phases 3 and 4 are clearly associated with the planarization of BD in its s-cis form. In phase 3, the BD C1C2C3C4 dihedral angle decreases from 29° to 16° forced by the increasing exchange repulsion of the approaching E. Actually, the electronic structure of BD resists the conformational change as is indicated by the negative C1C2C3C4 curvature component (thin black line in Figure 4). This component together with the C5C4 approach component is responsible for the curvature peak in phase 3. In phase 4, the rotation of BD into its s-cis form is accelerated (positive C1C2C3C4 curvature component, Figure 4) due to the formation of a distorted but fully conjugated BD, which finally adopts the s-cis planar form in phase 5. This planarization process is accompanied by the rotation of E at its C5C6 axis to become coplanar (Figure 1 and Table 2).

During phases 1 to 4, the C_1-symmetrical RC converts into a C_s-symmetrical one, which is reached at curvature minimum M5. Distances, which must become equivalent under C_s-symmetry

DOI: 10.1021/acs.jpca.5b11493
J. Phys. Chem. A 2016, 120, 1097–1111

Table 2. Energy and Geometry Changes along the Reaction Path Given for Each Phase[a]

curvature minimum M_n beginning of phase m	FP phase 1	M1 phase 2	M2 phase 3	M3 phase 4	M4 phase 5	M5 phase 6	M6 phase 7	TS	M7 phase 8	M8 phase 9	M9 phase 10
path parameter s	−17.71	−16.66	−14.74	−13.00	−10.42	−6.07	−3.16	0.00	0.84	3.5	6.19
energy change	0.08	0.08	0.18	0.51	1.09	3.27	8.98	19.91	17.10	−26	−38.99
in %	0.4	0.4	0.9	2.6	5.5	16.4 6	45.1	100	95.2	0	0
AB	3.93	3.91	3.78	3.63	3.43	2.98	2.59	2.14	2.02	1.42	1.42
ABC	104.27	109.42	113.35	114.80	112.58	107.36	110.79	118.87	120.86	133.97	134.53
DAB	158.67	155.74	149.11	140.00	117.81	94.77	93.22	102.62	107.23	122.94	123.07
EAB	21.29	24.22	30.76	39.79	61.62	85.56	90.52	103.27	108.27	120.45	120.53
DAE	179.96	179.94	179.85	179.79	179.73	179.67	176.26	154.11	144.50	116.61	116.40
γ = 180− (EAB + ABC)	54.44	46.36	35.89	25.41	5.80	−12.92	−21.31	−42.14	−49.13	−74.42	−75.06
EABC	5.63	5.59	2.30	0.21	0.00	0.00	−0.01	0.00	0.01	0.01	−0.14
C1C2C3C4	31.3	31.1	29.0	15.7	0.6	0	0	0	0	0	0

[a]Energies given in kcal/mol relative to the sum of energies of gauche 1,3-butadiene and ethene with BSSE-corrections included. The relative orientation of the reactants to each other is given by distance AB, bond angles ABC, etc., and dihedral angle EABC. For an explanation of the geometrical parameters, see Figure 1. Path parameter s in amu$^{1/2}$ Bohr, distances in Å, angles in degrees. A: midpoint of C5 and C6. B: midpoint of C1 and C4. C: midpoint of C2 and C3. D: midpoint of H7 and H15. E: midpoint of H8 and H16. FP: Fist point of the reaction path.

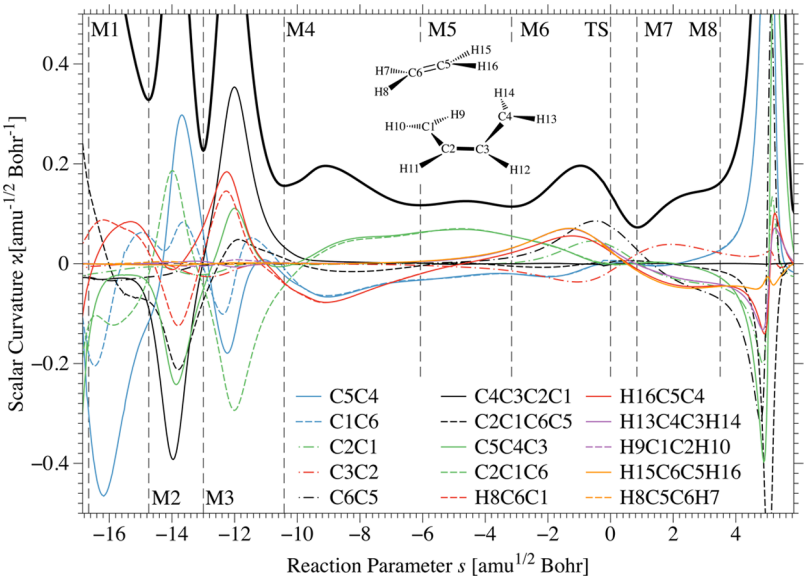

Figure 4. Scalar curvature (bold black line) of the Diels−Alder reaction between 1,3-butadiene and ethene is shown in enhanced form for the prechemical and chemical range. It is decomposed into internal coordinate contributions $k_m(s)$ (given in color as described in the legend).

seem to fulfill this criterion already at M4, but are not reliable. A more sensitive measure is provided by the curvature components such as C5C4C3 (solid green line in Figure 4) and C2C1C6 (dashed green line), which merge somewhat after M5 (Figure 2).

At s = −9.37 units, the two reactants are shortly in parallel planes but E is still shifted slightly to the exo side. Beyond this path point, E is tilted with its exo side downward (negative tilting angle γ, Table 2). The curvature maximum at s = −9.37 units specifies that point where the electrostatic attraction between the endo H atoms of E and the π-densities is weakened because of the continued rotation of E at its C5C6 axis.

The observation of distinct curvature peaks in the first five phases is unexpected in view of an energy increase of just 1.09 kcal/mol (5.5% of the activation energy; Table 2). For comparison, the internal rotation of ethane requires 3 kcal/mol and does not lead to any significant curvature along the "rotational path." However, conformational processes in a stable molecule and in a RC differ with regard to the energy valleys in which they take place. In the case of the ethane rotation the path is dominated by the dihedral angle. The internal rotation has little coupling with the bond lengths and the bending angles of the molecule. In the case of the RC of the DA reaction, the reaction path follows, after passing a valley-ridge inflection (VRI) point at s = −6.7 units on its way down from the TS toward the van der Waals region in the entrance channel, an energy ridge between two side-valleys. Because of the accuracy limitations of the calculations, there comes a point where the RC leaves the ridge path, curves down to a side valley, and then curves in the direction of the side valley. In this way, electronic structure changes are enhanced by the topology of the PES; i.e., the two curvature peaks in phases 3 and 4 correspond to BD planarization peaks, which are enhanced by the change from an unstable ridge path to a stable side-valley path.

Apart from this, it holds that even for a flat reaction valley any coupling between translational and vibrational motions leads to changes in the direction of the valley, i.e., to a curving

DOI: 10.1021/acs.jpca.5b11493
J. Phys. Chem. A 2016, 120, 1097−1111

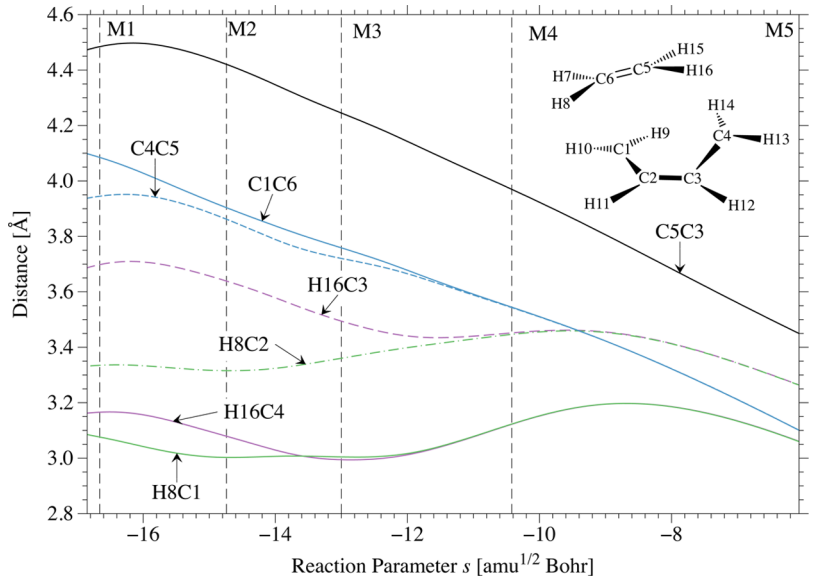

Figure 5. Changes in interatomic distances during the Diels–Alder reaction between 1,3-butadiene and ethene shown for the prechemical range of the reaction path. The reaction phases are indicated by dashed vertical lines at the positions of the curvature minima M1–M5.

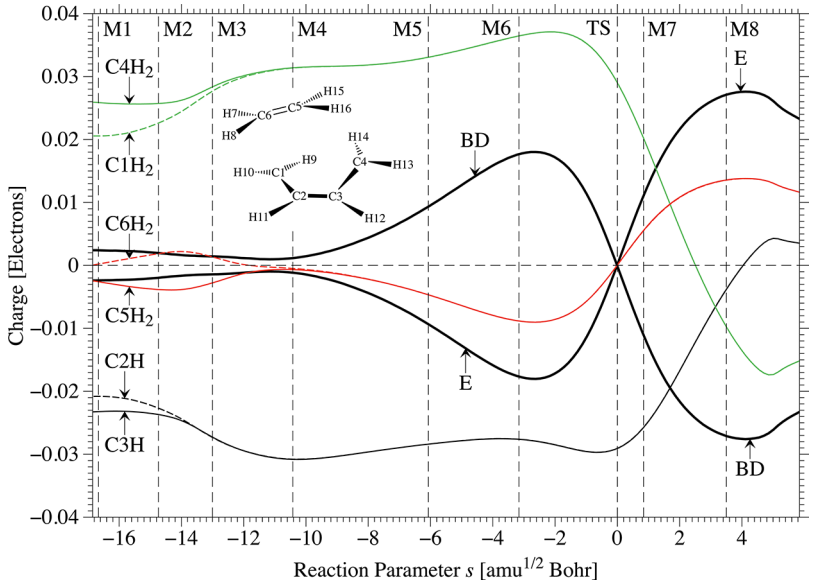

Figure 6. Charge transfer and changes in atom and group charges during the Diels–Alder reaction between 1,3-butadiene (BD) and ethene (E). The bold black lines give the charge of BD and E: The reaction phases are indicated by dashed vertical lines at the positions of the curvature minima M5–M8.

of the reaction path. Exchange repulsion, electrostatic, and/or dispersion interactions have a stronger impact on the path direction in a flat valley than in a valley with steep energy walls where polarization and rehybridization have to be initiated by a significant charge transfer. In the case of the DA reaction, the stereochemistry of a loosely bonded RC is strongly driven by exchange repulsion and whenever this increases or decreases, there is a change in the scalar curvature as for example in phase 2 (Figure 3).

The changes in exchange repulsion and charge polarization are reflected by the approach parameters C5C4 and C1C6 and the corresponding curvature components (solid and dashed blue lines in Figure 4, compare also with Figure 5). The curvature changes in the C5C4 component are always larger than those in the C1C6 component because the former distance is shorter (Figure 5) and therefore the changes in the exchange repulsion between C5 and C4 are larger (Figure 4). This is a consequence of the gauche form of BD given in Figure 1 in form of a right-handed helix for an assumed dienophile attack from above. There is a charge transfer of 3 me from BD to E (Figure 6), which plays a significant role in the orientation process. It preferentially takes place via a C4–C5 overlap and leads to a small polarization of E ($C5H_2$ is more negatively charged than $C6H_2$) and BD ($C4H_2$ is more positively charged than $C1H_2$ and C3H more negatively than C2H). Charge transfer and polarization facilitate the cis-rotation of BD under the exchange repulsion impact of E. It is telling that with the planarization of BD at M4 the charge transfer and polarization become minimal (Figure 6).

The cis-rotation of BD decreases the exchange repulsion and therefore a positive (supportive) C5C4 curvature component results in phase 3. Planarization involves an increased intramolecular

DOI: 10.1021/acs.jpca.5b11493
J. Phys. Chem. A 2016, 120, 1097–1111

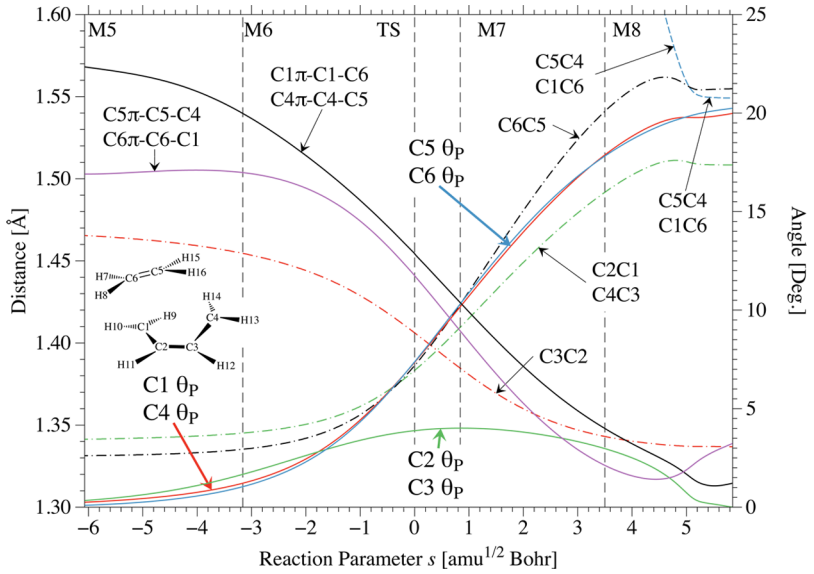

Figure 7. Changes in interatomic distances and pyramidalization angles θ_P during the Diels–Alder reaction between 1,3-butadiene and ethene. The reaction phases are indicated by dashed vertical lines at the positions of the curvature minima M1–M8. See text.

C2C3 antibonding overlap and increased exchange repulsion between the terminal groups and therefore the C1C2C3C4 component is resisting (negative). Together they are dominating the curvature peak in phase 3. In phase 4, their roles switch, but they are still responsible for the curvature peak in this region. At the end of phase 3, a bifurcation point is located (Figure 2), which cannot be accurately determined because the path taken from the TS into the entrance channel leaves the ridge path before the bifurcation point and continues in one of the side-valleys. The planarization of BD requires 1.09 kcal/mol, which is between the two values Craig and co-workers determined for the free gauche BD (0.51 more likely and 1.16 kcal/mol less likely).[17] During the orientation process, the approach distance AB becomes shorter and reaches between M3 and M4 the van der Waals distance of 3.6 Å between two C atoms interacting via their pπ-orbitals (see Figure 5). Electrostatic effects, as mentioned above, are responsible for the curvature peak in phase 5 (M4 to M5) and at the end of this phase, the VRI point and C_s-symmetry of the RC is reached as the side-valleys end in the main reaction valley leading to the TS.

Hence, the prechemical processes can be summarized as follows: phase 1, rotation (movement) of C6 toward C1 (0.4% energy increase, Table 2); phase 2, tilting of E and C4C5 approach (0.9%); phase 3, enforced first part of the planarization of BD caused by E-rotation at axis AB so that C5C6 and C1C4 become parallel (2.9%); phase 4, planarization of BD and tilting of the E-plane (5.5%); phase 5, reducing electrostatic attractions on the endo side of E by rotation at the C5C6 axis, with endo H atoms up and exo H atoms down (16.4% corresponding to 3.27 kcal/mol).

Chemical Processes (Reaction Phases 6–9). From M4 on, a new charge transfer period begins, which increases to a maximal value of 18 me transferred from BD to E at $s = -2.3$ units. This initiates the actual chemical processes taking place in phases 6 to 9. In phase 6, the charge transfer of 17 me from the HOMO(BD) to the LUMO(E) leads to a shortening of the C2C3 bond, a slight pyramidalization of the 4 terminal C atoms measured by the pyradimalization angle θ_P (Figure 7), a somewhat stronger pyramidalization at C2 and C3 (1.5 compared to 1°) and an orientation of the π-orbitals at C1 and C4 toward the incoming new bonding partners C6 and C5 (measured by the angles C1π–C1–C6 and C4π–C4–C5 (C$n\pi$ gives the end of the unit vector pointing into the direction of the π-orbital). These are all small changes as is the increase of the energy by just 5.7–8.9 kcal/mol (45.1% of the barrier value of 19.91 kcal/mol relative to the energy of the RC based on gauche BD; see Table 2), which indicates that the reactants slowly and steadily prepare for the reaction.

In phase 7, significant changes take place triggered by the continuing charge transfer to the LUMO(E), which adopts its maximum value and then decreases to zero at the TS located in this phase. The charge transfer facilitates pyramidalization and biradicaloid formation, which accelerates toward M7 and then slows down in phases 8 and 9 where pyramidalization reaches its maximum value of 20° with the new CC bond formation. Close to the TS, all CC bonds adopt a value of 1.397 Å (aromatization and bond equalization point). Phase 7 leads from an electrophilic attack of E against BD to a nucleophilic one (see Figure 6). The curvature maximum in phase 7 corresponds to the changes in the bond length components C5C6, C1C2, C3C4, and C2C3, which follow the curvature contribution due to pyramidalization (measured in Figure 4 by the angle contributions H8C5C6H7, H15C6C5H16, etc.).

While phase 7 is the rehybridization and aromatization phase, phase 8 (after the TS) is the biradicaloid formation phase, which implies the conversion of closed shell singlet π-electron pairs into open shell singlet pairs supported by the finalization of the pyramidalization of the terminal CH_2 groups of the reactants, which takes place for the four reacting centers at the same time. At the TS, pyramidalization has proceeded up to 35% ($\theta_P = 7°$), at M7 up to 50%, and at M8 up to 90%, and it is finalized with the bond formation in phase 9 (Figure 7). URVA reveals that just 35% of pyramidalization is sufficient for a decoupling of electron spin in the π-bonds of BD and E. An indication of the latter process is the recoupling of spin and the formation of the double bond C2C3 as indicated by the C2C3 curvature contribution (dot-dashed red line in Figure 4), which is responsible for the shoulder of the large C5C4/C1C6 bond formation curvature peak in phase 9. Also, in phase 8,

DOI: 10.1021/acs.jpca.5b11493
J. Phys. Chem. A 2016, 120, 1097–1111

the CC σ bond formations start, which increases the energy release in this phase, which together with the 2.8 kcal/mol in phase 7 amounts to 45.9 kcal/mol. This shows that energetically phase 8 (M7 to M8) is the phase in the exit channel where the largest energy release takes place.

The finalization of the CC single bond formations is indicated by the large curvature peak in phase 9 at s = 5.4 units (Figure 3). It is predominated by curvature contributions C4C5 and C1C6 as well as the angles C2C1C6 and C5C4C3, which are adjusted in the process of bond formation. This leads to a release of another 13 kcal/mol so that at M9 the boat form of cyclohexene is formed 58.9 kcal/mol down from the TS.

Role of the Transition State. The TS is important insofar as its energy influences the reaction rate and (more indirectly) the yield of the products. Furthermore, many chemists assume that the TS is also mechanistically relevant as it is the point where the chemical processes of bond breaking (forming) take place. Work carried out with the URVA method has shown that the TS is mechanistically often not relevant as the chemical processes take place before or after the TS.[39,40,43,44] The TS is just a PES point where the sum of all energy contributions, no matter whether important for the mechanism or not, leads to a saddle point of first order on the PES.

The curvature diagram in Figure 4 is in line with this interpretation as it clarifies that the mechanistically relevant point is M7 rather than the TS. However, the TS is important in another way. The charge transfer diagram of Figure 6 reveals that at the TS the distorted E (BD) converts from an electrophile (nucleophile) into a nucleophile (electrophile). This change can be traced back to a switch in the nature of the HOMO of the RC, which before the TS is predominantly the A″ HOMO of distorted BD and which after the TS, due to an allowed orbital energy crossing, is essentially the A′ HOMO of distorted E. This switch in the character of the HOMO results from the pyradimalization of the terminal CH_2 groups and the corresponding equalization of the three double bond lengths to a C1C6 (C4C5) distance of 2.268 Å when reaching the TS. This is in line with an early TS, which is shifted relative to the bond forming point at s = 5 units strongly into the entrance channel according to a quantified Hammond-Leffler postulate.[48,83−85]

The importance of the TS as charge-transfer switching point is a result of the energy-enforced C_s-symmetry of the RC. Mechanistically more important is M7 (the smallest curvature point in the investigated region) as this is the inflection point for the pyramidalization curves C1θ_P (C4θ_P) and C5θ_P (C6θ_P) (θ_P = 10.44° at M7), the corresponding curvature components, the bond length components, and the maximum of the pyramidalization angle C2θ_P (C3θ_P) (θ_P = 4.2° at M7, see Figure 7). The fact that M7 is already 2.8 kcal/mol downhill from the TS, shows that charge transfer drives and dominates the reaction. The reversion of the density flow (first from BD to E, then from E to BD) leads to the highest energy point along the reaction path.

According to the Dewar−Evans−Zimmerman rules, the TS of the DA reaction involves six electrons, is Hückel aromatic, and is therefore stabilized.[25] The equalization of the CC bonds, observed in this and in previous work,[34] confirms the aromatic character of the TS although it occurs somewhat after rather than exactly at the TS (Figure 7). Sakai[35] assessed the aromatic character of the TS using a CI (configuration interaction) description based on localized orbitals and deriving an aromaticity index from the weights of those CI terms, which describe singlet coupling and polarization of each CC bond. According to his results, the aromaticity of the TS of the DA reaction is comparable with that of benzene. Cossio and co-workers[31] summarized the criteria by which electron delocalization in a pericyclic TS can be estimated. For the DA reaction, an aromatic stabilization energy of up to 10 kcal/mol was estimated[37] (5.7 kcal/mol estimated by Doering and co-workers;[32] 2.3−7.7 kcal/mol by Goldstein and co-workers[33]). A diamagnetic exaltation Λ of −14.0 ppm cgs[36] and a NICS (nucleus-independent chemical shift) value at the TS of −19.4 ppm[31,36] also speaks of a substantial aromatic character of the TS.

Postchemical Processes (Reaction Phases 10 and 11). In these phases, the cyclohexene boat is converted into its halfchair form via ring pseudorotation, which leads to an energy release of 5.1 kcal/mol. In Figure 8, the conformational globe for a six-membered ring as given by Cremer and Pople (CP)[18] is shown for cyclohexene with planar cyclohexene being positioned at the origin of the globe. The conformational space of any 6-membered ring is spanned by 3 curvilinear (puckering) coordinates, which can be derived as hypercylindrical coordinates spanning the equator plane of the CP globe by the puckering amplitude q_2 (degree of puckering) and the pseudorotational phase angle ϕ_2 (type of puckering), which runs from 0 to 360°. This is indicated for cyclohexene in steps of 30° in Figure 8 (at 0, 60, 120, etc., boat forms; at 30, 90, 150, etc., twistboat forms; note that there are an infinite number of intermediate forms). The third coordinate is the puckering amplitude q_3, which defines chair (north pole, $q_3 > 0$) and inverted chair form (south pole, $q_3 < 0$).[18]

Ring inversion via planar cyclohexene requires 10 kcal/mol and is not the preferred process as the planar form sits at a second order saddle point. Lower energy forms of cyclohexene lie on an ellipsis (Figure 8), which cuts the globe into two equivalent halves. The latter are populated by high-energy forms caused by a distortion of the double bond, decoupling of the π-electrons, and biradical character. Along the elliptic path on the globe surface the boat forms of cyclohexene are TSs of ring pseudorotation. For the DA reaction, they correspond to the bifurcation points BP1 and BP2 shown in Figure 8. (In a similar way, one can explain the existence of two bifurcation points for the retro-DA reaction close to M5. See Figure 9.)

At the start of the pseudorotation path (s = 5.8 units), the BP leads to a large curvature peak, which indicates the topology of the PES rather than a large electronic structure change (the path curves at BP in two different directions; Figures 3 and 8). The shoulder of this peak is associated with the change in the boat form along the pseudorotation path, which implies the reduction of a relatively large puckering amplitude (Q = 0.610 Å). In phase 11, an envelope form with 5 atoms in a common plane is generated (Figure 8). When in phase 11 the half-chair is reached, the curvature is relatively small (Figure 3) according to a smaller Q value of 0.479 Å.

4. CHEMICAL RELEVANCE OF THE URVA ANALYSIS

The study carried out in this work is based on the assumption that one representative reaction path (e.g., the IRC path) is sufficient to elucidate the mechanism of the corresponding chemical reaction. However, a chemical reaction is a stochastic event, which may follow in the time average a different reaction mechanism than that resulting from the analysis of a representative path, which is constrained to a concerted, synchronous cycloaddition as done in the URVA analysis. Reaction dynamical

DOI: 10.1021/acs.jpca.5b11493
J. Phys. Chem. A 2016, 120, 1097−1111

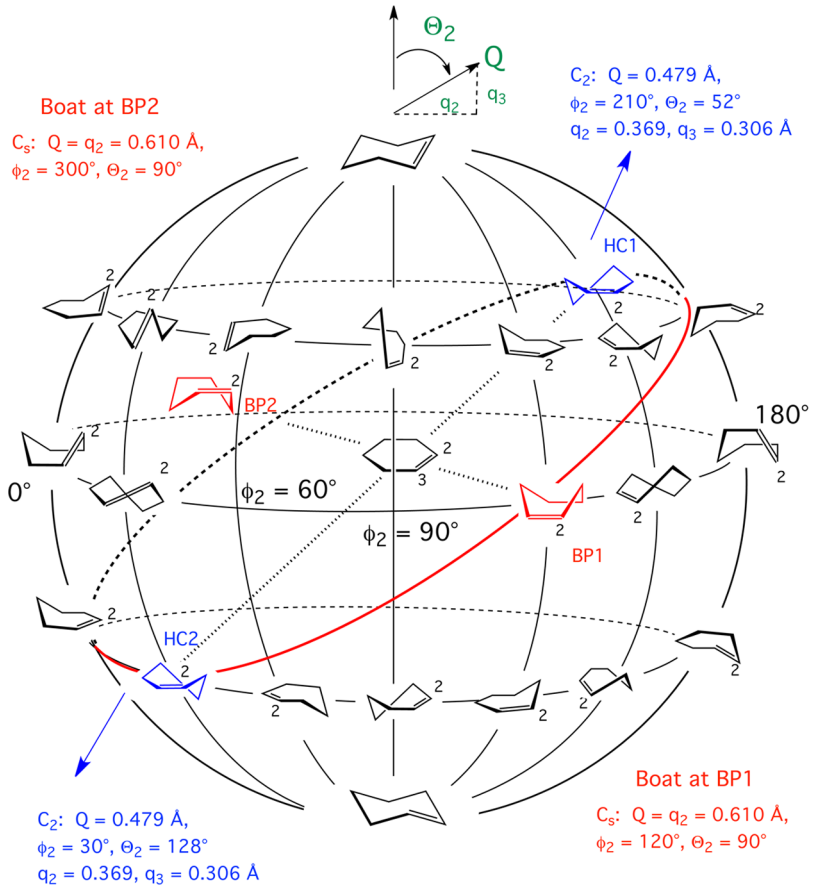

Figure 8. Conformational globe of cyclohexene. The ring pseudorotation path of cyclohexene generated as boat form at a bifurcation point (BP1 or BP2, red) of the DA reaction to the stable half-chair (HC1 or HC2 in blue) is indicated by the bold red (front of globe) and black dashed lines (back of globe). The calculated puckering parameters are also given in hyper cylindrical coordinates q_2, ϕ_2, q_3 or the corresponding spherical coordinates Q, ϕ_2, Θ_2.[18]

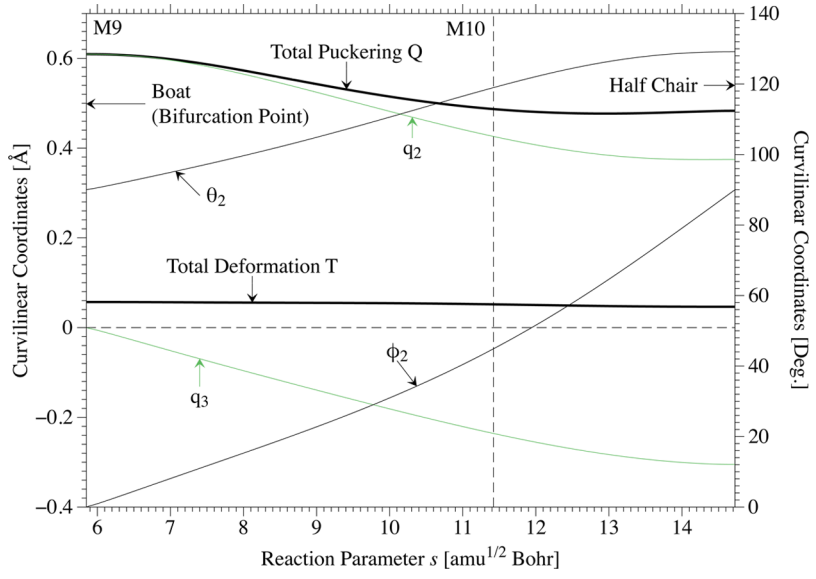

Figure 9. Change in puckering coordinates for the conversion of the boat form of cyclohexene generated at the bifurcation point (BP) of the DA reaction into the stable half-chair (HC) form. For an explanation of the puckering parameters, see text. The pseudorotation phase angle ϕ_2 is given as $\phi_2 + 90°$ to simplify the diagram. Boat and half-chair form correspond to BP2 and HC2 in Figure 8. Also given is the total deformation amplitude T in Å[75] of cyclohexene, which does not change.

studies are available to scrutinize this assumption. Houk and co-workers investigated the DA reaction by employing quasiclassical trajectory calculations, wich were initialized at the saddle point by TS-normal mode sampling.[86] In this way,

DOI: 10.1021/acs.jpca.5b11493
J. Phys. Chem. A 2016, 120, 1097−1111

information about the time gap between the first and second CC bond formation is obtained.[19] These authors found for the symmetrical DA reactions of butadiene, cyclopentadiene, and cyclohexadiene with ethylene or acetylene average time gaps of 5 fs or less between the formation of the two new CC bonds at 298 K. These time gaps are all shorter than a CC bond vibrational period (ca. 30−60 fs),[87] thus identifying these reactions as following a synchronous concerted mechanism. Even for the asymmetric DA reaction between 2-hydroxybutadiene and cyanoacetylene, 97% of trajectories were still concerted, e.g., leading directly to the DA product, whereas only 3% involved biradical intermediates at 298 K. At high temperatures (up to 1180 K) only 2% of the trajectories for the symmetric reactions invoked a biradical intermediate indicating an asynchronous mechanism.[19] This is in line with results obtained by Hratchian and Schlegel, who found in a reaction dynamics study based on a damped classical trajectory algorithm that the symmetric DA reaction follows paths closely resembling the IRC path.[22] Hence it is justified to conclude that the mechanism of the symmetric DA reaction is even at higher temperatures reasonably described by using the IRC path at 0 K, which necessarily leads to a synchronous concerted mechanism.

According to the Woodward and Hoffmann rules, the parent DA reaction in its concerted form is a symmetry-allowed $\pi^4s + \pi^2s$ cycloaddition and does not lead to any symmetry-induced increase in the barrier.[24,88] Investigations based on state function and orbital symmetries,[24] frontier molecular orbital (FMO) theory[26] in connection with perturbational MO (PMO) theory,[27] conceptual DFT,[5,30] aromaticity models of the TS,[31] or an analysis based on electron localization functions (ELF)[29] all predict a relatively low barrier for the parent DA reaction and are able to predict changes in the barrier upon substitution of diene or dienophile.

The convincing success of the orbital analysis of the DA reaction in its many forms becomes understandable by the URVA analysis. The 11-phase mechanism of the parent DA reaction is complex where especially the five prechemical and two postchemical phases complicate the mechanism because these phases correspond to different symmetries of the RC and therefore also to different interaction patterns between the reactants (Figure 3). The prechemical and chemical regions are charge transfer-driven whereas ring pseudorotation in the postchemical region is strain-driven (relaxation to the halfchair form of cyclohexene).

At first sight, the curvature diagram does not provide any hint on the position of the TS. This is clearly provided by the charge transfer curves in Figure 6, which cross at the TS. The charge transfer from BD to E is the prerequisite for the formation of the new CC bonds. It leads to the pyramidalization of the CH_2 groups in connection with rehydrization at the C atoms, the decoupling of spins, and the formation of two biradicaloids that can react with each other. The increasing charge transfer is facilitated by the continuous approach of the two reactants, which costs energy. There is a direct relationship between the energy curve of Figure 2, the charge transfer curves in Figure 6, and the curvature diagrams in Figures 3 and 4. Where the maximum of the charge transfer curve (transfer of 18 me from BD to E; $s = -2.6$ s-units) is reached, the energy curve has an inflection point; i.e., the energy increase slows down from this point on for increasing s. At the position of the energy maximum the charge transfer becomes zero and the switch in the role of diene and dienophile as donor and acceptor of charge occurs (Figure 6).

Exactly at the TS, there is a switch in the A''-symmetrical HOMO of the RC (dominated by π_2 of BD) with the A'-symmetrical HOMO−1 (dominated by the π_1 of BD) because the HOMO gains C1C6- and C1C5-σ-character and is accordingly stabilized. The HOMO − 1 becomes the ethene π-bonding orbital from which charge is donated into the A'-symmetrical π_3(BD) orbital facilitating the formation of the new C2C3 double as well as the C1C2 and C3C4 single bonds in the BD-part of the RC.

Since the charge transfer in the RC of the DA reaction depends on the energy of the frontier orbitals, i.e. the HOMO of the diene and the LUMO of the dienophile in the current case, it is straightforward to predict the influence of heteroatoms, substituents, or the conformation of the RC on the height of the barrier or the stereo- and regiochemistry of the reaction. This explains the success of FMO, PMO, or other orbital based theories when predicting features of the mechanism of DA reactions.

URVA indicates the position of the TS by the fact that the two major approach components, C1C6 and C4C5, pass from a resisting to a supporting approach (Figure 4). Apart from this it is noteworthy that at the TS only 35% of the pyramidalization of the terminal methylene groups ($\theta_P = 7°$) is carried out in the RC. The increase of the pyramidalization angle from 7 to 20° produces rather than requires energy. This implies that a relatively small degree of pyramidalization leads to an effective spin-decoupling of the π-electrons, which become available for the recoupling with other electrons in the form of the new CC bonds as confirmed by the σ-character of the HOMO at the TS.

Because of a substantial improvement of the URVA method with regard to both its valley-following algorithm, the decomposition of the scalar curvature into internal coordinate components, and the use of curvilinear coordinates, the prechemical, chemical, and postchemical phases of the DA reaction have been analyzed and an 11-phase mechanism has been established, by following the RC far out into the entrance and exit channel beyond the bifurcation points that lead to the C_1- and C_2-symmetrical RC. The observed mechanism can be characterized as follows. The prechemical phases involve reactant orientation, diene planarization, and RC symmetrization; the chemical phases involve charge-transfer and diene polarization, pyramidalization at the terminal C atoms, bond equalization, and biradicaloid and CC bond formation; the postchemical phases involve ring pseudorotation from boat to halfchair via an envelope form. The following URVA-based insights have been gained.

(1) The curvature of the reaction path reflects the electronic structure changes of the RC and the topology of the PES. The latter becomes relevant when the reaction path bifurcates. The position of the bifurcation point is indicated by bifurcation peaks of the curvature.
(2) We have distinguished two different bifurcation points, which appear in different regions of the PES. (a) If the latter is flat, a VRI point precedes the bifurcation point, which is connected to the former by an energy ridge path. Since the limits in the accuracy of the path following algorithm lead to a loss of the ridge path and a *curving down* to a side valley with subsequent *curving* into the direction of the side-valley path, the bifurcation of the ridge path is announced by curvature peaks that can be

DOI: 10.1021/acs.jpca.5b11493
J. Phys. Chem. A 2016, 120, 1097−1111

related to electronic structure changes and that can be relatively large because they are enhanced by the topology of the PES. (b) If the PES is steep, the valley bifurcation point is reached without any a priori *warning* by a VRI; i.e., ridge path and side-valleys do not exit in this case. Also, in this case, it is possible to set up the path following algorithm in such a way that it does not stop at the bifurcation point. Then, the approximate position of the bifurcation point is given by a *bifurcation peak* of the curvature (see Figure 3).

(3) Conformational changes such as the internal rotation of a molecule do no lead to path curvature because there is minimal coupling between path following and vibrational motions, which is the dynamic prerequisite of path curving. However, conformational or configurational changes of the RC taking place in the pre- or post-chemical region lead to distinct curvature peaks when they involve electronic structure changes initiated, e.g., by charge transfer and charge polarization. Since the reaction valley is rather flat in these areas, even small changes in the electronic structure can lead to a curving of the path and thereby significant curvature enhancements. This is exploited in the URVA analysis of the reaction mechanism.

(4) For the first time, the URVA analysis of the parent DA reaction gives a detailed description of the mechanistic processes taking place in the pre- and postchemical phases. It is surprising that these processes are also driven by charge transfer and charge polarization in close relationship to what happens in the chemical phases.

(5) The planarization of gauche BD, even though it requires just 1.1 kcal/mol (easily available if the BD molecule surmounts the anti-gauche barrier of 5.7 kcal/mol[17]), takes place in two distinct reaction phases. In the first, the angle C1C2C3C4 is forced from 29 to 16° by exchange repulsion and in the second from 16 to 1° driven by an improved 4π-delocalization. This is initiated by a 3 me charge transfer from BD to E.

(6) The plane of E is always tilted with regard to that of BD where it is first endo tilted to avoid exchange repulsion and to benefit from H,C attraction. Later, it is exo tilted to enable charge transfer via FMO interactions but keeping the exchange repulsion low. The rotation of E from the endo tilted into the exo tilted form is reflected by a distinct curvature peak at −9.5 *s*-units.

(7) The changes of the RC up to its point of symmetrization require just 3.3 kcal/mol, 2.6 kcal/mol of which are still available from surmounting the trans−gauche barrier of BD. From thereon the concerted and collective change of all geometry parameters requires just another 16.6 kcal/mol due to a 6.5 kcal/mol aromatic stabilization of the TS, which is not available for the biradical mechanism.[8,21]

(8) Charge transfer of maximal 18 me and C1C2 (C4C3) charge polarization by 30−37 me are sufficient to start pyramidalization and subsequent bond equalization. These are the driving forces for the concerted DA reaction. However, one has to see them as a consequence of the symmetrization of the RC geometry, which in turn is the result of an interplay between a minimal initial charge transfer, exchange repulsion, electrostatic attraction, and enforced BD planarization. In this sense, it is justified to say that the fate of the concerted DA reaction is already decided during the pericyclic approach mode of BD and E.

(9) The TS of the DA reaction between BD and E is the point where the reaction partners switch their roles as electrophilic (first E, then BD) or nucleophilic agent, which is the result of an allowed crossing of the FMOs. This crossing directly follows from the C_s symmetry of the RC. At the TS, neither pyramidalization at the reacting C atoms nor bond equalization is completed. In this regard, the curvature minimum M7 would be a much more useful mechanistic reference point because from there on pyramidalization and bond changes become accelerated.

(10) The results of the URVA analysis strongly suggest that the TS is stabilized due to the quantum mechanical effect of aromatization by this benefiting from an estimated stabilization energy of 6.5 kcal/mol. Therefore, the TS is shifted into the entrance channel by as much as 5 *s*-units relative to the center of the CC bond formation point at s = 5 units in line with the quantified Hammond−Leffler postulate[48,85] and confirmed by the unusually long CC interaction distances of 2.268 Å, which normally adopt values of 1.9−2.0 Å in TSs involving CC bond formation.

(11) The biradicaloid formation is finalized in phase 8 as is indicated by the finalization of the C2C3 double bond and the immediate formation of the CC single bonds. The latter is facilitated by the fact that the biradicaloids of BD and E are simultaneously generated. Phase 8 has an energy release of 45.9 kcal/mol.

(12) The finalization of the CC single bonds takes place in phase 9 as indicated by the large curvature peak dominated by the C1C6 and C4C5 curvature components. The finalization leads to another release of 13 kcal/mol. The remaining 5.1 kcal/mol are released when the halfchair form of cyclohexene is formed.

(13) The retro-DA reaction is characterized by a large curvature peak at s = 5 units, which indicates a sudden change after forcing cyclohexene into the boat form so that density of the double bond can be transferred into the σ^* orbitals of C1C6 and C4C5. Clearly, this charge transfer is facilitated by substituents at C1 and C4, which facilitate the charge transfer process and thereby C1C6 and C4C5 bond cleavage.

(14) In view of the high activation energy for the retro DA reaction (64 kcal/mol), an enforced but also controlled cleavage of cyclohexene might be possible by fine-tuning a Laser on the C1C6 and C4C5 stretching vibrations. However, the analysis of Coriolis couplings (not discussed) reveals that three avoided crossings of the stretching mode before the TS of the retro DA reaction lead to dissipation of energy in the RC rather than bond breaking.

Beyond these specific insights, the URVA analysis provides for the first time a full account on the reaction mechanism thus being able to predict, confirm, complement, or detail mechanistic features some of which have been already obtained by other approaches such as the orbital analysis.

(i) Any structural stabilization of the diene in a syn-form as in cyclopentadiene or o-quinodimethane shortens the pre-chemical phase and thereby a lowers the barrier by 2 kcal/mol. This is in line with the activation enthalpies found for the DA reaction of cyclopentadiene with ethene (22.6 compared to 24.8 kcal/mol).[80] (ii) A higher barrier for the formation of the

DOI: 10.1021/acs.jpca.5b11493
J. Phys. Chem. A 2016, 120, 1097−1111

gauche form of the diene will increase the probability of a two-step mechanism via a biradical. The gauche form of the diene leads to a right-handed (or left-handed) helix of the RC in the entrance channel, which will be helpful in connection with chiral synthesis.[89] (iii) The URVA analysis reveals that already for the parent DA reaction the RC is sensitive to interactions of the endo positioned H atoms with the π-density of BD. It is easy to foresee that substituents with π-orbitals will enhance these interactions and lead to a distinctive difference between endo- and exo-orientation of the dienophile. (iv) Early in the entrance channel, the RC has C_1-symmetry, which leads to an asynchronous approach between C1,C6 and C4,C5. Any substituent that enforces asynchronicity in the chemical phases will cause two separated curvature peaks for C1C6 and C4C5 bond formation. The *s*-distance between the peaks will be a quantitative measure for the asynchronicity of bond formation. (v) Rate enhancement of the DA reaction is achieved by increasing the charge transfer from diene to dienophile, which is accomplished by electron-donating groups for the former and electron-withdrawing groups for the latter.[1−5] Catalysis of the DA reaction is possible by increasing the effect of the withdrawing groups, which can be achieved by suitable Lewis acids such as BF_3.[3,9−13] (vi) The parent DA reaction has in water a higher barrier (0.71 kcal/mol, PCM calculations). Charge transfer and charge polarization in the parent DA reaction is too small to establish H-bonding between water and the dienophile. The prerequisite of the water catalysis discussed in the literature[51−53] is the presence of a polar group in the RC that can interact with water via H-bonding. The latter will have the electronic effect of increased charge transfer from diene to dienophile thus lowering the barrier. It will be difficult to separate the electronic effect from the predicted effect of enforced hydrophobicity.[51−53] Clearly, space confinement will lower the barrier as this forces the reaction partners together. However, enforced hydrophobicity in water does not play any role for the parent reaction as is indicated by the increase rather than the decrease in the barrier.

By providing a deep insight into the mechanistic features of the parent DA reaction, the basis is laid to carry out URVA analyses for substituted dienes and dienophiles and Lewis-acid catalyzed and hetero DA reactions.

■ ASSOCIATED CONTENT

Supporting Information

The Supporting Information is available free of charge on the ACS Publications website at DOI: 10.1021/acs.jpca.5b11493.

Harmonic vibrational frequencies and avoided crossings for the retro Diels-Alder reaction as a function of the reaction parameter s, additional curvature, energy, and geometry diagrams, Ball&Stick representations of the reaction complex at selected points along the reaction path and the corresponding Cartesian Coordinates are given. (PDF)

■ AUTHOR INFORMATION

Corresponding Author

*(D.C.) E-mail: dcremer@smu.edu. Telephone: 01-214-768-1300.

Notes

The authors declare no competing financial interest.

■ ACKNOWLEDGMENTS

We thank Dr. W. Zou and Dr. M. Freindorf for useful comments on this project. This work was financially supported by the National Science Foundation, Grants CHE 1152357 and CHE 1464906. We thank SMU for providing computational resources.

■ REFERENCES

(1) Beusker, P. H.; Scheeren, H. W. Intermolecular cyclization reactions to form carbocycles. In *The Chemistry of Dienes and Polyenes*; Wiley: 2000; Chapter 5, pp 329−479.

(2) Wittkopp, A.; Schreiner, P. R. Catalysis of Diels-Alder reactions in water and in hydrogen-bonding environments In *The Chemistry of Dienes and Polyenes*; Wiley: 2000; Chapter 13, pp 1029−1088.

(3) Fringuelli, F.; Taticchi, A. *The Diels Alder Reaction: Selected Practical Methods*; Wiley: Chichester, 2002.

(4) Morgan, K. M. Reaction Mechanisms Part (iii) Pericyclic Reactions. *Annu. Rep. Prog. Chem., Sect. B: Org. Chem.* **2003**, *99*, 378−395.

(5) Ess, D. H.; Jones, G. O.; Houk, K. N. Conceptual, Qualitative, and Quantitative Theories of 1,3-Dipolar and Diels-Alder Cycloadditions Used in Synthesis. *Adv. Synth. Catal.* **2006**, *348*, 2337−2361.

(6) Rowley, D.; Steiner, H. Kinetics of Diene Reactions at High Temperatures. *Discuss. Faraday Soc.* **1951**, *10*, 198−213.

(7) Houk, K. N.; Gonzalez, J.; Li, Y. Pericyclic Reaction Transition States: Passions and Punctilios, 1935−1995. *Acc. Chem. Res.* **1995**, *28*, 81−90.

(8) Lischka, H.; Ventura, E.; Dallos, M. The Diels-Alder Reaction of Ethene and 1,3-Butadiene: An Extended Multireference ab initio Investigation. *ChemPhysChem* **2004**, *5*, 1365−1371.

(9) Yates, P.; Eaton, P. Acceleration of the Diels-Alder Reaction by Aluminum Chloride. *J. Am. Chem. Soc.* **1960**, *82*, 4436−4437.

(10) Fringuelli, F.; Taticchi, A. *Dienes in the Diels-Alder Reaction*; Wiley: New York, 1990.

(11) Carruthers, W. *Cycloaddition Reactions in Organic Synthesis*; Pergamon Press: Oxford, U.K., 1990.

(12) Garcia, J. I.; Martinez-Merino, V.; Mayoral, J. A.; Salvatella, L. Density Functional Theory Study of a Lewis Acid Catalyzed Diels-Alder Reaction. The Butadiene + Acrolein Paradigm. *J. Am. Chem. Soc.* **1998**, *120*, 2415−2420.

(13) Yamabe, S.; Minato, T. A Three-Center Orbital Interaction in the Diels-Alder Reactions Catalyzed by Lewis Acids. *J. Org. Chem.* **2000**, *65*, 1830−1841.

(14) Papies, O.; Grimme, W. Acceleration of the (4 + 2)-Cycloreversion by the Alkoxide Substituent. *Tetrahedron Lett.* **1980**, *21*, 2799−2802.

(15) Lewis, D. K.; Bergmann, J.; Manjoney, R.; Paddock, R.; Kalra, B. L. Rates of Reactions of Cyclopropane, Cyclobutane, Cyclopentene, and Cyclohexene in the Presence of Boron Trichloride. *J. Phys. Chem.* **1984**, *88*, 4112−4116.

(16) Ichihara, A. Retro-Diels-Alder Strategy in Natural Product Synthesis. *Synthesis* **1987**, *1987* (3), 207−222.

(17) Boopalachandran, P.; Craig, N.; Groner, P.; Laane, J. Gas-Phase Raman Spectra and the Potential Energy Function for the Internal Rotation of 1,3-Butadiene and Its Isotopologues. *J. Phys. Chem. A* **2011**, *115*, 8920−8927.

(18) Cremer, D.; Pople, J. A. A General Definition of Ring Puckering Coordinates. *J. Am. Chem. Soc.* **1975**, *97*, 1354−1358.

(19) Black, K.; Liu, P.; Xu, L.; Doubleday, C.; Houk, K. N. Dynamics, Transition States, and Timing of Bond Formation in Diels-Alder Reactions. *Proc. Natl. Acad. Sci. U. S. A.* **2012**, *109*, 12860−12865.

(20) Gayatari, G. Performance of ab initio and DFT Methods in Modeling Diels-Alder Reactions. *Indian J. Chem., Sect. A: Inorg., Bioinorg., Phys., Theor. Anal. Chem.* **2011**, *50A*, 1579−1586.

(21) Isobe, H.; Takano, Y.; Kitagawa, Y.; Kawakami, T.; Yamanaka, S.; Yamaguchi, K.; Houk, K. N. Extended Hartree-Fock (EHF) Theory of Chemical reactions VI: Hybrid DFT and post-Hartree-Fock

DOI: 10.1021/acs.jpca.5b11493
J. Phys. Chem. A 2016, 120, 1097−1111

Approaches for Concerted and Non-concerted Transition Structures of the Diels-Alder Reaction. *Mol. Phys.* **2002**, *100*, 717−727.
(22) Hratchian, H. P.; Schlegel, H. B. Following Reaction Pathways Using a Damped Classical Trajectory Algorithm. *J. Phys. Chem. A* **2002**, *106*, 165−169.
(23) Huang, C.-H.; Tsai, L.-C.; Hu, W.-P. Dual-Level Direct Dynamics Study on the Diels-Alder Reaction of Ethylene and 1,3-Butadiene. *J. Phys. Chem. A* **2001**, *105*, 9945−9953.
(24) Woodward, R. B.; Hoffmann, R. *The Conversation of Orbital Symmetry*; Verlag Chemie: Weinheim, Germany, 1970.
(25) Dewar, M. Aromaticity and Pericyclic Reactions. *Angew. Chem., Int. Ed. Engl.* **1971**, *10*, 761−776.
(26) Fleming, I. *Frontier Orbitals and Organic Chemical Reactions*; Wiley: Chichester, U.K., 1976.
(27) Dewar, M. J. S.; Dougherty, R. C. *The PMO Theory of Organic Chemistry*; Plenum Press: New York, 1975.
(28) Houk, K. N.; Strozier, R. W. Lewis Acid Catalysis of Diels-Alder Reactions. *J. Am. Chem. Soc.* **1973**, *95*, 4094−4096.
(29) Berski, S.; Andres, J.; Silvi, B.; Domingo, L. R. The Joint Use of Catastrophe Theory and Electron Localization Function to Characterize Molecular Mechanisms. A Density Functional Study of the Diels-Alder Reaction between Ethylene and 1,3-Butadiene. *J. Phys. Chem. A* **2003**, *107*, 6014−6024.
(30) De Proft, F.; Ayers, P. W.; Fias, S.; Geerlings, P. Woodward-Hoffmann Rules in Density Functional Theory: Initial Hardness Response. *J. Chem. Phys.* **2006**, *125*, 214101.
(31) Arrieta, A.; de Cozar, A.; Cossio, F. P. Cyclic Electron Delocalization in Pericyclic Reactions. *Curr. Org. Chem.* **2011**, *15*, 3594−3608.
(32) Doering, W. v. E.; Roth, W. R.; Breuckmann, R.; Figge, L.; Lennartz, H.-W.; Fessner, W.-D.; Prinzbach, H. Verbotene Reaktionen. - [2 + 2]-Cycloreversion Starrer Cyclobutane. *Chem. Ber.* **1988**, *121*, 1−9.
(33) Goldstein, E.; Beno, B.; Houk, K. N. Density Functional Theory Prediction of the Relative Energies and Isotope Effects for the Concerted and Stepwise Mechanisms of the Diels-Alder Reaction of Butadiene and Ethylene. *J. Am. Chem. Soc.* **1996**, *118*, 6036−6043.
(34) Kraka, E.; Wu, A.; Cremer, D. Mechanism of the Diels-Alder Reaction Studied with the United Reaction Valley Approach: Mechanistic Differences between Symmetry-allowed and Symmetry-forbidden Reactions. *J. Phys. Chem. A* **2003**, *107*, 9008−9021.
(35) Sakai, S. Theoretical Study on the Aromaticity of Transition States in Pericyclic Reactions. *J. Phys. Chem. A* **2006**, *110*, 6339−6344.
(36) Chen, Z.; Wannere, C. S.; Corminboeuf, C.; Puchta, R.; Schleyer, P. v. R. Nucleus-Independent Chemical Shifts (NICS) as an Aromaticity Criterion. *Chem. Rev.* **2005**, *105*, 3842−3888.
(37) Bachrach, S. M.; White, P. B. Towards Assessing the Aromaticity of the Diels-Alder Transition State. *J. Mol. Struct.: THEOCHEM* **2007**, *819*, 72−78.
(38) Konkoli, Z.; Cremer, D.; Kraka, E. Unified Reaction Valley Approach: Mechanism of the Reaction $CH_3 + H_2 \Rightarrow CH_4 + H$. *J. Phys. Chem. A* **1997**, *101*, 1742−1757.
(39) Kraka, E.; Cremer, D. Computational Analysis of the Mechanism of Chemical Reactions in Terms of Reaction Phases: Hidden Intermediates and Hidden Transition State. *Acc. Chem. Res.* **2010**, *43*, 591−601.
(40) Cremer, D.; Kraka, E. From Molecular Vibrations to Bonding, Chemical Reactions, and Reaction Mechanism. *Curr. Org. Chem.* **2010**, *14*, 1524−1560.
(41) Cremer, D.; Wu, A.; Kraka, E. The mechanism of the reaction $FH+H_2C = CH_2 \Rightarrow H_2C\text{-}CFH_3$. Investigation of Hidden Intermediates with the Unified Reaction Valley Approach. *Phys. Chem. Chem. Phys.* **2001**, *3*, 674−687.
(42) Konkoli, Z.; Cremer, D. A New Way of Analyzing Vibrational Spectra I. Derivation of Adiabatic Internal Modes. *Int. J. Quantum Chem.* **1998**, *67*, 1−9.
(43) Kraka, E. Reaction Path Hamiltonian and the Unified Reaction Valley Approach. *WIREs Comp.l Mol. Sci.* **2011**, *1*, 531−556.
(44) Kraka, E. In *Encyclopedia of Computational Chemistry*; Schleyer, P., Allinger, N., Clark, T., Gasteiger, J., Kollman, P., Schaefer, H., III, Schreiner, P., Eds.; Wiley: Chichester, U.K., 1998; Vol. *4*; pp 2437−2463.
(45) Zou, W.; Sexton, T.; Freindorf, M.; Kraka, E.; Cremer, D. A New Method for Describing the Mechanism of a Chemical Reaction based on the Unified Reaction Valley Approach. *J. Chem. Theory Comput.* **2016**, DOI: 10.1021/acs.jctc.5b01098.
(46) Joo, H.; Kraka, E.; Quapp, W.; Cremer, D. The Mechanism of a Barrierless Reaction: Hidden Transition State and Hidden Intermediate in the Reaction of Methylene with Ethene. *Mol. Phys.* **2007**, *105*, 2697−2717.
(47) Kraka, E.; Joo, H.; Cremer, D. A Stunning Example for a Spontaneous Reaction with a Complex Mechanism: The Vinylidene-Acetylene Cycloaddition Reaction. *Mol. Phys.* **2010**, *108* (19−20), 2667−2685.
(48) Kraka, E.; Zou, W.; Freindorf, M.; Cremer, D. Energetics and Mechanism of the Hydrogenation of XH_n for Group IV to Group VII Elements X. *J. Chem. Theory Comput.* **2012**, *8*, 4931−4943.
(49) Freindorf, M.; Sexton, T.; Kraka, E.; Cremer, D. The Mechanism of the Cycloaddition Reaction of 1,3-Dipole Molecules with Acetylene: An Investigation with the Unified Reaction Valley Approach. *Theor. Chem. Acc.* **2014**, *133*, 1423.
(50) Cremer, D.; Szabo, K. J. In *Methods in Stereochemical Analysis, Conformational Behavior of Six-Membered Rings, Analysis, Dynamics, and Stereoelectronic Effects*; Juaristi, E., Ed.; VCH Publishers: 1995; pp 59−134.
(51) Rideout, D. C.; Breslow, R. Hydrophobic Acceleration of Diels-Alder Reactions. *J. Am. Chem. Soc.* **1980**, *102*, 7816−7817.
(52) Breslow, R. Hydrophobic Effects on Simple Organic Reactions in Water. *Acc. Chem. Res.* **1991**, *24*, 159−164.
(53) Breslow, R.; Zhu, Z. N. Quantitative Antihydrophobic Effects as Probes for Transition State Structures. 2. Diels-Alder Reactions. *J. Am. Chem. Soc.* **1995**, *117*, 9923−9924.
(54) Miller, W.; Handy, N.; Adams, J. Reaction Path Hamiltonian for Polyatomic Molecules. *J. Chem. Phys.* **1980**, *72*, 99−112.
(55) Konkoli, Z.; Cremer, D. A New Way of Analyzing Vibrational Spectra III. Characterization of Normal Vibrational Modes in Terms of Internal Vibrational Modes. *Int. J. Quantum Chem.* **1998**, *67*, 29−41.
(56) Kraka, E.; Larsson, J.; Cremer, D. In *Theoretical and Computational Chemistry, Vol. 5, Theoretical Organic Chemistry, C.*; Parkanyi, C., Ed.; Elsevier: Amsterdam, 1998; pp 259−327.
(57) Kraka, E.; Larsson, J.; Cremer, D. In *Vibrational Modes in Computational IR Spectroscopy*; Grunenberg, J., Ed.; Wiley: New York, 2010; pp 105−149.
(58) Raghavachari, K.; Trucks, G. W.; Pople, J. A.; Head-Gordon, M. A Fifth-Order Perturbation Comparison of Electron Correlation Theories. *Chem. Phys. Lett.* **1989**, *157*, 479−483.
(59) Dunning, T. J. Gaussian Basis Sets for Use in Correlated Molecular Calculations I. The Atoms Boron Through Neon and Hydrogen. *J. Chem. Phys.* **1989**, *90*, 1007−1023.
(60) Becke, A. D. Density-Funcitonal Thermochemistry. III. The Role of Exact Exchange. *J. Chem. Phys.* **1993**, *98*, 5648−5652.
(61) Stephens, P. J.; Devlin, F. J.; Chabalowski, C. F.; Frisch, M. J. Ab initio calculation of Vibrational Absorption and Circular Dichroism Spectra Using Density Functional Force Fields. *J. Phys. Chem.* **1994**, *98*, 11623−11627.
(62) Hariharan, P.; Pople, J. The Influence of Polarization Functions on Molecular orbital Hydrogenation Energies. *Theor. Chim. Acta* **1973**, *28*, 213−222.
(63) Chai, J.-D.; Head-Gordon, M. Systematic Optimization of Long-range Corrected Hybrid Density Functionals. *J. Chem. Phys.* **2008**, *128*, 084106.
(64) Chai, J.-D.; Head-Gordon, M. Long-range Corrected Hybrid Density Functionals with Damped AtomÐAtom Dispersion Corrections. *Phys. Chem. Chem. Phys.* **2008**, *10*, 6615−6620.
(65) Boys, S.; Bernardi, F. The Calculation of Small Molecular Interactions by the Differences of Separate Total Energies. Some Procedures with Reduced Errors. *Mol. Phys.* **1970**, *19*, 553−566.

DOI: 10.1021/acs.jpca.5b11493
J. Phys. Chem. A 2016, 120, 1097−1111

(66) Fukui, K. The Path of Chemical Reactions - the IRC Approach. *Acc. Chem. Res.* **1981**, *14*, 363−368.
(67) Quapp, W.; Kraka, E.; Cremer, D. Finding the Transition State of Quasi-barrierless Reactions by a Growing String Method for Newton Trajectories: Application to the Dissociation of Methylenecyclopropene and Cyclopropane. *J. Phys. Chem. A* **2007**, *111*, 11287−11293.
(68) Hratchian, H. P.; Schlegel, H. B. Accurate Reaction Paths Using a Hessian based Predictor-Corrector Integrator. *J. Chem. Phys.* **2004**, *120*, 9918−9924.
(69) Hratchian, H. P.; Frisch, M. J.; Schlegel, H. B. Steepest Descent Reaction Path Integration Using a First-order Predictor-Corrector Method. *J. Chem. Phys.* **2010**, *133*, 224101.
(70) Hratchian, H. P.; Schlegel, H. B. Using Hessian Updating To Increase the Efficiency of a Hessian Based Predictor-Corrector Reaction Path Following Method. *J. Chem. Theory Comput.* **2005**, *1*, 61−69.
(71) Hratchian, H. P. Using Efficient Predictor-Corrector Reaction Path Integrators for Studies Involving Projected Frequencies. *J. Chem. Theory Comput.* **2012**, *8*, 5013−5019.
(72) Hratchian, H. P.; Kraka, E. Improved Predictor-Corrector Integrators For Evaluating Reaction Path Curvature. *J. Chem. Theory Comput.* **2013**, *9*, 1481−1488.
(73) Reed, A.; Curtiss, L.; Weinhold, F. Intermolecular Interactions from a Natural Bond Orbital, Donor-Acceptor Viewpoint. *Chem. Rev.* **1988**, *88*, 899−926.
(74) Weinhold, F.; Landis, C. R. *Valency and Bonding: A Natural Bond Orbital Donor-Acceptor Perspective*; Cambridge University Press: 2003.
(75) Zou, W.; Izotov, D.; Cremer, D. New Way of Describing Static and Dynamic Deformations of the Jahn-Teller Type in Ring Molecules. *J. Phys. Chem. A* **2011**, *115*, 8731−8742.
(76) Kraka, E.; Zou, W.; Filatov, M.; Gräfenstein, J.; Gauss, J.; He, Y.; Wu, A.; Konkoli, Z.; He, Z.; Cremer, D. et al., *COLOGNE15*; 2015.
(77) Werner, H. J.; Knowles, P. J.; Kniza, G.; Manby, F. R.; Schütz, M.; et al. *MOLPRO*, version 2010.1, A Package of ab initio Programs. 2010; see http://www.molpro.net, last access date: Octber 30, 2015.
(78) Frisch, M. J.; Trucks, G. W.; Schlegel, H. B.; Scuseria, G. E.; Robb, M. A.; Cheeseman, J. R.; Scalmani, G.; Barone, V.; Mennucci, B.; Petersson, G. A. et al.; *Gaussian 09*, Revision C.01. 2010.
(79) Pieniazek, S. N.; Houk, K. N. The Origin of the Halogen Effect on Reactivity and Reversibility of Diels-Alder Cycloadditions Involving Furan. *Angew. Chem., Int. Ed.* **2006**, *45*, 1442−1445.
(80) Guner, V.; Khuong, K. S.; Leach, A. G.; Lee, P. S.; Bartberger, M. D.; Houk, K. N. A Standard Set of Pericyclic Reactions of Hydrocarbons for the Benchmarking of Computational Methods: The Performance of ab Initio, Density Functional, CASSCF, CASPT2, and CBS-QB3Methods for the Prediction of Activation Barriers, Reaction Energetics, and Transition State Geometries. *J. Phys. Chem. A* **2003**, *107*, 11445−11459.
(81) Cox, J. D.; Pilcher, G. *Thermochemistry of Organic and Organometalic Compounds*; Academic Press: London, 1970.
(82) Lide, D. R. *CRC Handbook of Chemistry and Physics*, 90th ed.; CRC: Boca Raton, FL, 2009−2010.
(83) Hammond, G. A Correlation of Reaction Rates. *J. Am. Chem. Soc.* **1955**, *77*, 334−338.
(84) Leffler, J. Parameters for the Description of Transition States. *Science* **1953**, *117*, 340−341.
(85) Cremer, D.; Kraka, E. Verification and Quantification of the Hammond-Leffler Postulate. *Rev. Proc. Quim.* **2012**, *2012*, 27−30.
(86) Bolton, K.; Hase, W. L.; Peslherbe, G. H. In *Modern Methods for Multidimensional Dynamics Computation in Chemistry*; Thompson, L., Ed.; World Scientific: Singapore, 1998; pp 143−189.
(87) Levin, R. *Molecular Reaction Dynamics*; Cambridge Univ Press: Cambridge, U.K., 2005.
(88) Woodward, R. B.; Hoffmann, R. The Conservation of Orbital Symmetry. *Angew. Chem., Int. Ed. Engl.* **1969**, *8*, 781−853.
(89) Ahrendt, K. A.; Borths, C. J.; MacMillan, D. W. C. New Strategies for Organic Catalysis: The First Highly Enantioselective Organocatalytic Diels-Alder Reaction. *J. Am. Chem. Soc.* **2000**, *122*, 4243−4244.

DOI: 10.1021/acs.jpca.5b11493
J. Phys. Chem. A 2016, 120, 1097−1111